Articles

The Role of Ca^{2+}-Coordinating Residues of Herring Antifreeze Protein in Antifreeze Activity†

Zhengjun Li,‡,§ Qingsong Lin,‡,§ Daniel S. C. Yang,|| K. Vanya Ewart,⊥ and Choy L. Hew*,‡,§

Division of Structural Biology, Hospital for Sick Children, and Departments of Laboratory Medicine and Pathobiology and of Biochemistry, University of Toronto, Toronto, Ontario, Canada, Department of Biological Sciences, National University of Singapore, Singapore, Department of Biochemistry, Faculty of Health Science, McMaster University, Hamilton, Ontario, Canada, and NRC Institute for Marine Biosciences, Halifax, Nova Scotia, Canada

Received July 16, 2004; Revised Manuscript Received September 3, 2004

ABSTRACT: The type II antifreeze protein of Atlantic herring (*Clupea harengus harengus*) requires Ca^{2+} as a cofactor to inhibit the growth of ice crystals. On the basis of homology modeling with Ca^{2+}-dependent lectin domains, five residues of herring antifreeze protein (hAFP) are predicted to be involved in Ca^{2+} binding: Q92, D94, E99, N113, and D114. The role of E99, however, is less certain. A previous study on a double mutant EPN of hAFP suggested that the Ca^{2+}-binding site of hAFP was the ice-binding site. However, it is possible that Ca^{2+} might function distantly to affect ice binding. Site-directed mutagenesis was performed on the Ca^{2+}-coordinating residues of hAFP in order to define the location of the ice-binding site and to explore the role of these residues in antifreeze activity. Properties of the mutants were investigated in terms of their structural integrity and antifreeze activity. Equilibrium dialysis analysis demonstrated that E99 is a Ca^{2+}-coordinating residue. Moreover, proteolysis protection assay revealed that removal of Ca^{2+} affected the conformation of the Ca^{2+}-binding loop rather than the core structure of hAFP. This finding rules out the possibility that Ca^{2+} might act at a distance via a conformational change to affect the function of hAFP. Substitutions at positions 99 and 114 resulted in severely reduced thermal hysteresis activity. These data indicate that the ice-binding site of hAFP is located at the Ca^{2+}-binding site and the loop region defined by residues 99 and 114 is important for antifreeze activity.

An important adaptation that allows many organisms to survive in ice-laden environments is the production of antifreeze glycoproteins (AFGPs)[1] or antifreeze proteins (AFPs). These macromolecular antifreezes depress the freezing temperature of body fluids in a noncolligative manner without significantly altering the melting temperature and protect organisms from freezing to death during periods of <0 °C (*1*). The difference between the melting and freezing temperatures is termed thermal hysteresis, which is widely used as an indicator of antifreeze activity.

There are five types of fish AF(G)Ps: AFGP and type I−IV AFPs (*1*, *2*). Although these proteins have a common feature to inhibit ice crystal growth, they are structurally diverse and bind to their specific ice crystal planes (*3*−*5*). Type II AFPs are Cys-rich globular proteins of molecular mass from 14 to 24 kDa, which are found in herring (*Clupea harengus harengus*), smelt (*Osmerus mordax*), and sea raven (*Hemitripterus americanus*) (*6*−*9*). These AFPs show no homology to other AFPs, but they are homologous to the carbohydrate-recognition domain of Ca^{2+}-dependent (C-type) lectins and adopt similar three-dimensional folds (*8*, *10*, *11*). An unusual feature of herring AFP (hAFP) and smelt AFP is that their antifreeze activity is Ca^{2+}-dependent, while the activity of sea raven AFP is Ca^{2+}-independent (*8*, *9*). Unlike type I and type III AFPs, the ice-binding sites (IBSs) and ice-binding residues of type II AFPs have not been determined yet. Although mutagenesis studies have been performed on sea raven AFP, the findings only suggest that its IBS is distinct from the Ca^{2+}-binding site (CaBS) of C-type lectins (*12*). Therefore, it is still uncertain where the IBS of sea raven AFP is located. In this study, the terms IBS and ice-binding residue will continue to be used to describe the protein surface and residues important for antifreeze activity despite the fact that the AFP does not interact with ice

† This work was supported by grants from the Canadian Institutes of Health Research (formerly the Medical Research Council, Canada) (to C.L.H.). Z.L. and Q.L. were supported by a Connaught Scholarship and a University of Toronto Open Fellowship. Q.L. was also supported by a RESTRACOM Fellowship, Hospital for Sick Children, Toronto.

* To whom correspondence should be addressed at the Department of Biological Sciences, National University of Singapore, Singapore 119260. Tel: (65) 6874-2692. Fax: (65) 6779-2486. E-mail: dbshead@nus.edu.sg.

‡ Hospital for Sick Children and University of Toronto.

§ National University of Singapore.

|| McMaster University.

⊥ NRC Institute for Marine Biosciences.

[1] Abbreviations: AFP, antifreeze protein; AFGP, antifreeze glycoprotein; CaBS, Ca^{2+}-binding site; CaCR, Ca^{2+}-coordinating residue; C-type lectin, Ca^{2+}-dependent lectin; hAFP, herring antifreeze protein; IBS, ice-binding site; MBP, mannose-binding protein.

10.1021/bi048485h CCC: $27.50
Published on Web 10/30/2004

molecules directly but with water molecules at the ice−water interface.

Based on the homology modeling with Ca^{2+}-dependent lectin domains from rat mannose-binding protein (MBP) and E-selectin, the structure of hAFP can be divided into two parts (*11*). The lower two-thirds portion is comprised mostly of elements of regular secondary structures, including β-sheets, two helices, and the N- and C-termini. The upper one-third structure contains a Ca^{2+}-binding loop (*11*). That the IBS of hAFP might be located at the CaBS is based on the study of the double mutant QPD → EPN, which changed residues at positions 92 and 94 of wild-type hAFP from the motif typical of galactose-binding C-type lectins to that more typical of mannose-binding lectins (*13*). This EPN (Q92E/D94N) mutant retained Ca^{2+} binding, while exhibiting dramatically reduced thermal hysteresis activity (*14*). Furthermore, observations that substitution of Ca^{2+} with other divalent metal ions decreased the activity of hAFP and altered ice crystal morphology also implied that the CaBS of hAFP might be directly involved in ice binding (*11*). However, the possibility that Ca^{2+} binding might affect ice binding at a distance via a conformational change in hAFP could not be completely ruled out. Residues Q92, D94, E99, N113, and D114 are predicted to be Ca^{2+}-coordinating residues (CaCRs) on the basis of the homology model of hAFP (*11*). However, the Ca^{2+}-coordinating role of E99 is less certain. hAFP might adopt either a coordination array similar to MBP which involves E99 as a CaCR or an alternative coordination pattern present in E-selectin which excludes E99 as a CaCR (*15*, *16*).

If the ice-binding surface of hAFP is located at the CaBS, it seems logical to propose that CaCRs of hAFP would be ice-binding residues as the corresponding residues contribute to carbohydrate binding in the C-type lectins. In this study, the role of CaCRs in hAFP was investigated to demonstrate that CaBS is the IBS and to determine how changes of the Ca^{2+}-coordinating geometry would affect ice−hAFP interaction. All CaCRs were substituted individually by Ala residues and other amino acids. A double mutant E99Q/N113D, which mutated E99 and N113 simultaneously to Gln and Asp residues, respectively, was also generated. The effects of side-chain substitutions on the function of hAFP were determined by examining thermal hysteresis and ice crystal morphology. Structural properties of the mutants were investigated using a variety of biophysical and enzymatic methods. It was observed that E99 is a CaCR, similar to the Ca^{2+} coordination array of MBP and not E-selectin. We also found that the removal of Ca^{2+} did not affect the basic fold of hAFP, but a conformational change occurred in the Ca^{2+}-coordinating loop. This finding excludes the possibility that Ca^{2+} might function at a distance to affect antifreeze activity via a conformational change and thus demonstrates that the IBS is located at the CaBS. Two of the CaCRs, E99 and D114, were identified to be essential for hAFP to inhibit ice crystal growth. This result suggests that the loop region defined by these two residues, rather than the whole Ca^{2+}-binding loop, is critical for ice binding.

EXPERIMENTAL PROCEDURES

Materials. Nickel nitrilotriacetic acid−agarose was purchased from Qiagen (Valencia, CA). Ruthenium red was from Fluka (St. Louis, MO). Prestained protein molecular mass standards were from Invitrogen (Carlsbad, CA). Endoproteinase Glu-C was obtained from Roche Molecular Diagnostics (Laval, Quebec, Canada). $^{45}CaCl_2$ was purchased from ICN Biomedicals (Irvine, CA). The dispo-equilibrium dialyzer was from AmiKa (Columbia, MD). All other chemicals were of reagent grade.

Generation, Expression, and Purification of hAFP Mutants. PCR was used to construct all mutants by the modified procedure of Aiyar and Leis (*17*), using the sense primer A 5′-GGCCGAATTCGCTGATGAATGTCCCACTGATTGG-AAG-3′ and the antisense primer B, which contained a mutation-specific sequence for each mutant to amplify the first PCR product. Several of mutagenic primers contained newly introduced restriction enzyme sites together with the mutated sequence in order to facilitate the subsequent screening of the mutants. The sense primer C 5′-ACAGATTGC CAAGTGTCAACC-3′ and the antisense primer D 5′-CTA-GTCTAGATCAATGGTGATGGTGATGGTGTTTCAGT-GGCTTGGCGCA-3′ were used to produce the second PCR product. The whole sequence of the hAFP gene was generated by using the two PCR products as templates and primers A and D. The final PCR product was subcloned into the pGAPZα A vector (Invitrogen). Mutant E99Q/N113D, which included two single-site changes at different positions, was generated by repeating PCR mutagenesis after the single mutant E99Q was available. Double mutant EPN, which mutated residues Gln at position 92 and Asp at position 94, was also cloned into the pGAPZα A vector from the previous construct using the pQE8 vector (*14*). All mutant clones were then confirmed by direct dideoxy sequencing. The constructs were transformed into yeast *Pichia pastoris* and expressed (*18*). Expressed proteins were detected by the tricine SDS−PAGE and Western blot using rabbit anti-hAFP antiserum as described previously (*18*).

Mutants were purified by nickel nitrilotriacetic acid−agarose affinity chromatography and by HPLC using a reverse-phase C4 column, as previously described (*18*). The concentrations of the hAFP protein samples were determined spectrophotometrically by using the molar extinction coefficient $\epsilon = 3.79 \times 10^4\ M^{-1}\ cm^{-1}$ determined as described by Mach et al. (*19*).

$^{45}CaCl_2$ Overlay and Ruthenium Red Staining. For the $^{45}CaCl_2$ binding study, hAFP and its mutants were run on the nonreducing tricine SDS−PAGE and electrophoretically transferred to 0.2 μm nitrocellulose membranes. The membranes were labeled with $^{45}CaCl_2$ containing 1 mCi/L $^{45}CaCl_2$ according to the procedure of Maruyama et al. (*20*). After autoradiography the membranes were stained with Ponceau S.

For ruthenium red staining, purified recombinant hAFP and its mutants were run on the nonreducing tricine SDS−PAGE following previously published procedures (*11*).

Proteolysis Protection Assay. A proteolysis protection assay was performed as previously described on hAFP and its mutants in 20 mM Tris-HCl, pH 8.0, with 1 mM $CaCl_2$ or 5 mM EDTA, containing 0.2 mg/mL endoproteinase Glu-C for 1 h at 21 °C (*11*). The reaction mixtures were resolved on the nonreducing tricine SDS−PAGE and stained with Coomassie Brilliant Blue.

Thermal Hysteresis Measurement and Ice Crystal Morphology. Thermal hysteresis of hAFP and its mutants was

Table 1: Equilibrium Dialysis Assay of hAFP and Its CaCR Mutants

hAFP	protein concn (μM)	K_d (μM)
WT-6H	45.2	34.2 ± 0.2
Q92A	461.8	$(1.14 \pm 0.03) \times 10^3$
D94A	523.3	$(1.76 \pm 0.04) \times 10^3$
E99A	430.2	$(1.37 \pm 0.02) \times 10^3$
N113A	377.2	741.3 ± 12.0
D114A	865.6	$(5.10 \pm 0.20) \times 10^3$
E99Q	104.3	200.3 ± 2.4
E99Q/N113D	36.2	13.6 ± 0.3
EPN	77.9	125.3 ± 1.4

measured by using a nanoliter osmometer (Clifton Technical Physics, Hartford, NY) as described by Chakrabartty et al. (*21*). Measurements for each sample were performed in triplicate from three different sample wells. All measurements were made in 40 mM Tris-HCl and 50 mM $CaCl_2$, pH 7.5. Ice crystal images were captured by video microscopy.

Ca^{2+}-Binding Affinity Analysis. Inactive apo-hAFPs were generated after purification by reverse-phase C4 HPLC. All buffers used were treated with Chelex 100 columns (Bio-Rad Laboratories, Mississauga, Ontario, Canada) to be metal-free and stored in plastic tubes. To facilitate the comparison of the different roles of five CaCRs, this analysis and the following two experiments focused on all five Ala mutants.

Equilibrium dialysis of hAFPs was performed with the dispo-equilibrium dialyzers with the two chambers separated by a dialysis membrane with a molecular mass cutoff of 5 kDa. The upper chamber of each dialyzer was filled with 75 μL of the protein sample containing 40 mM Tris-HCl and 150 mM NaCl, pH 7.5 (buffer A). The protein concentrations of apo-hAFP and its mutants are shown in Table 1. The lower chamber was filled with 75 μL of buffer A with 2.5 μCi/mL $^{45}CaCl_2$ in 250 μM $CaCl_2$. Equilibrium was reached in 24 h at 4 °C as judged by equal amounts of radioactivity in a pair of chambers containing $^{45}CaCl_2$ and lysozyme, respectively. Duplicate aliquots (20 μL) from each chamber were added to 15 mL of Biofluor liquid scintillation cocktail (Packard Instrument Co., Meriden, CT). The radioactivity from each chamber was counted in a LKB Wallac 1219 Rackbeta liquid scintillation counter. Nonspecific binding was estimated and subtracted by using lysozyme as a substitution of hAFP. The concentrations of the mutants after equilibrium were determined by the Bradford protein assay kit (Bio-Rad Laboratories). Triplicate samples were used for all measurements.

Hydrogen−Deuterium Exchange Studies of Ala Mutants. The concentrations of stock solutions of hAFP and its Ala mutants were 1 mg/mL in 20 mM NH_4OAc and 20 mM $CaCl_2$, pH 7.0. Hydrogen−deuterium exchange was initiated by diluting the protein sample 20-fold in D_2O, incubating for 2 h at 4 °C, and freezing by dry ice before use. The final D_2O concentration of all samples was 95%. Unexchanged hAFP (0% deuterium exchange control) and completely deuterium-exchanged hAFP (100% deuterium exchange control) were analyzed with each set of samples to determine the amount of deuterium. The unexchanged hAFP and its mutants were prepared by mixing their stock solutions with H_2O. Completely deuterium-exchanged samples were prepared by incubating hAFPs in D_2O with 10% formic acid at 90 °C for 5 h. All samples were examined by Q-TOF electrospray ionization mass spectrometry (Advanced Protein Technology Centre, Hospital for Sick Children, Toronto, Ontario, Canada).

Intrinsic Fluorescence of Ala Mutants. Steady-state fluorescence of hAFP mutants was measured at room temperature using a QM-1 fluorescence spectrophotometer (Photon Technology International, Lawrenceville, NJ) equipped with excitation intensity correction and a magnetic stirrer. For measurements of the fluorescence, emission spectra from 300 to 400 nm were collected at 1 nm intervals with the excitation wavelength set at 280 nm. Slit widths were 5 nm for both excitation and emission. A quartz cuvette with 1 cm path length and 0.5 mL volume was used. Spectra of buffer only or buffer with Ca^{2+} were used to correct for light scattering. For the Ca^{2+}-modulated conformational studies of Ala mutants, spectra of apo-hAFPs in 40 mM Tris-HCl, pH 7.5, with or without 50 mM $CaCl_2$ were achieved. Relative fluorescence intensity was obtained by using the maximum fluorescence intensity of hAFP in the absence of Ca^{2+} as 100%. The protein concentrations used were 0.60 μM for wild-type hAFP, 0.61 μM for Q92A, 0.63 μM for D94A, 0.63 μM for E99A, 0.59 μM for N113A, and 0.60 μM for D114A, respectively. These protein concentrations were within the range of 0.2−0.9 μM, in which the relationship of different protein concentrations of hAFP and the fluorescence intensity was linear. The inner filter or the protein aggregation effect would not significantly affect the measurements within this range.

RESULTS

Expression and Purification of hAFP Mutants Corresponding to CaCRs. hAFP mutants were expressed in *P. pastoris*. All five amino acid residues involved in the Ca^{2+} coordination were mutated individually by altering the charge property or the length of the side chain. Western blot analysis indicated that all 18 mutants generated could be expressed in *P. pastoris* (data not shown). However, the expression level of mutant D94N was much lower than other mutants due to the introduction of an N-glycosylation site which resulted in the formation of glycosylated hAFP with a higher molecular mass. All mutants were expressed and purified by nickel affinity column and reverse-phase C4 HPLC.

$^{45}CaCl_2$ Overlay Assay. To verify that hAFP mutants did not disrupt protein folding and Ca^{2+} binding, Ca^{2+}-binding properties of all mutants were tested by the $^{45}CaCl_2$ overlay method and by ruthenium red staining for some mutants (Figure 1). All mutants bound Ca^{2+} properly, suggesting that substitution of one of the CaCRs did not dramatically alter the geometry of Ca^{2+} coordination. Weaker $^{45}CaCl_2$-binding bands, such as D94A (Figure 1A), appeared to result from the lower protein concentration rather than the weaker Ca^{2+}-binding ability as indicated by the parallel experiment of Ponceau S staining (Figure 1B). Ruthenium red staining shown in Figure 1D further confirmed that D94A could bind Ca^{2+}.

Proteolysis Protection Assay. hAFP undergoes conformational change and becomes protease-resistant upon Ca^{2+} binding (*11*). Proteolysis protection assay was performed on all hAFP mutants to evaluate their conformations and Ca^{2+}-binding abilities (Figure 2). Resistance to Glu-C digestion in the presence of 1 mM Ca^{2+} further confirmed that all mutants bound Ca^{2+}, a result that was similar to that of wild-

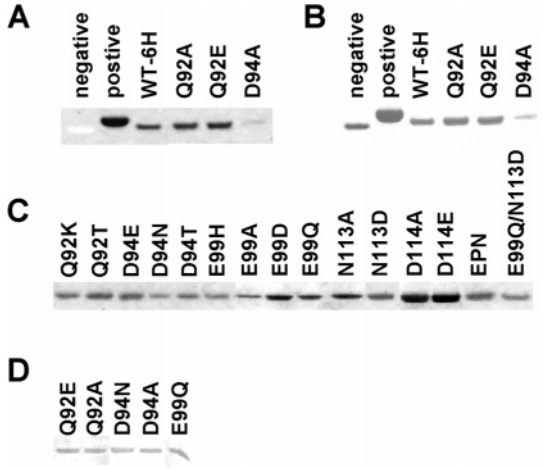

FIGURE 1: Ca^{2+}-binding properties of hAFP and its CaCR mutants. (A) $^{45}CaCl_2$ overlay assay of wild-type hAFP WT-6H, mutants Q92A, Q92E, and D94A, and its related Ponceau S staining in (B). Lysozyme was used as a negative control, and β-lactoglobulin was used as a positive control. (C) $^{45}CaCl_2$ overlay assay of hAFP mutants Q92K, Q92T, D94E, D94N, D94T, E99H, E99A, E99D, E99Q, N113A, N113D, D114A, D114E, EPN, and E99Q/N113D. (D) Ruthenium red staining of hAFP CaCR mutants Q92E, Q92A D94N, D94A, and E99Q.

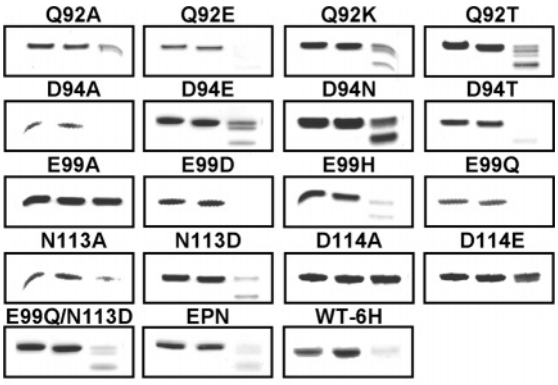

FIGURE 2: Proteolysis protection assay of hAFP and its CaCR mutants. Endoproteinase Glu-C was used to detect the conformational change of the hAFPs in the presence and absence of Ca^{2+}. Upon Ca^{2+} binding, hAFPs were resistant to digestion. For each protein sample (from left to right), the first lane represented the protein alone, and the second lane and the third lane were proteins with or without Ca^{2+} in the presence of Glu-C, respectively. The lower bands of the second and the third lanes compared with the first one were due to the removal of part of the N-terminal amino acids as explained previously (*18*).

type hAFP. All mutants except E99A and D114A were degraded in the absence of Ca^{2+}. Resistance of mutants E99A and D114A to proteolysis even in the absence of Ca^{2+} suggested that the initial protease-sensitive site of hAFP was located within the region where these amino acid residues were mutated. Therefore, residues E99 and D114 were most susceptible to Glu-C digestion. The proteolysis protection study implied that at least one residue, either E99 or D114, should be available for Glu-C cleavage in order to further degrade hAFP in the absence of Ca^{2+}. However, the reason both E99A and D114A were resistant to proteolysis in the absence of Ca^{2+} will require further structural information. One interpretation is that substitutions of Glu or Asp to Ala could change the hydrophobicity of the Ca^{2+}-binding loop. Consequently, in the absence of Ca^{2+}, a relatively compact

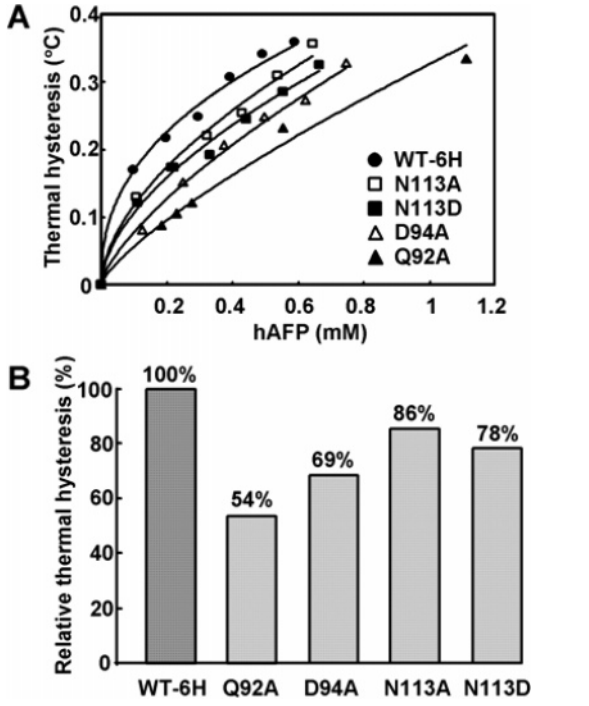

FIGURE 3: Thermal hysteresis activity of hAFP and its CaCR mutants Q92A, D94A, N113A, and N113D. (A) Measurements of concentration-dependent thermal hysteresis of wild-type hAFP WT-6H and its mutants. (B) Relative thermal hysteresis of hAFP CaCR mutants (0.4 mM) compared with that of WT-6H.

conformation resistant to proteolysis, similar to that of the Ca^{2+}-bound form, was produced.

Thermal Hysteresis Measurement and Ice Crystal Morphology. Antifreeze activities of all hAFP mutants were determined by measuring thermal hysteresis. Taking into consideration the different Ca^{2+} affinity of each mutant, all measurements were conducted at 50 mM Ca^{2+}, which was at least 10-fold higher than the measured K_d determined by equilibrium dialysis analysis. Thermal hysteresis curves were obtained for those mutants with measurable activity (Figure 3A). Relative thermal hysteresis of these mutants (0.4 mM) compared with wild-type hAFP was also shown (Figure 3B).

One characteristic of AF(G)Ps is that they can alter ice crystal morphology. In a "normal" condition where AF(G)P is absent, ice growth forms a circular disklike crystal (Figure 4A, buffer) (*22*). In the presence of AF(G)P, these molecules can bind to the prism faces, and the ice crystal can be modified from a circular plate to a columnar spicule or to the hexagonal bipyramidal ice crystal, depending on the AF(G)P concentration (*23*). Therefore, for mutants with no measurable thermal hysteresis activity, the ability to alter the shape of ice growth was accessed and compared. The effects of the mutation on hAFP antifreeze activity were classified into four groups on the basis of their ice crystal morphology (Figure 4).

Comparison of relative thermal hysteresis activity of the Ala-mutated CaCRs (Figure 3B) showed that five CaCRs contributed differently to the activity. Mutant N113A had 86% of the wild-type hAFP activity, followed by mutants D94A and Q92A, which retained 69% and 54% activity, respectively. In contrast, both E99 and D114 hAFP mutants were shown to be important for antifreeze activity. Mutant

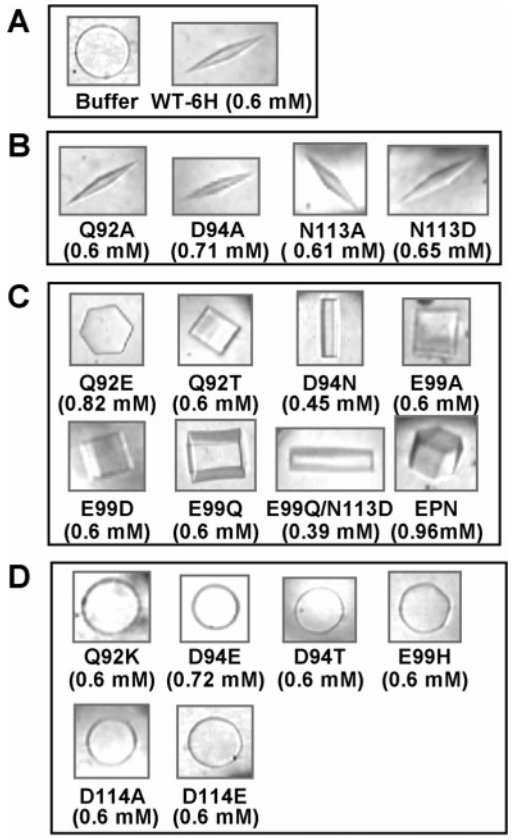

FIGURE 4: Ice crystal morphology of hAFP and its CaCR mutants. The samples were (A) buffer alone and wild-type hAFP WT-6H, (B) hAFP mutants with reduced thermal hysteresis, (C) hAFP mutants which retained the ability to modify the ice crystal with no detectable thermal hysteresis, and (D) hAFP mutants that completely lost thermal hysteresis. The protein concentrations used for each sample are indicated.

E99A only modified the ice crystal with no detectable thermal hysteresis activity, and D114A was devoid of any thermal hysteresis (Figures 3B and 4). The N113 mutants showed only a slight decrease in thermal hysteresis, suggesting that this CaCR is relatively less critical for ice binding. Activity measurement for the double mutant E99Q/N113D showed normal Ca^{2+}-binding affinity with no detectable thermal hysteresis. It is noted that mutant EPN showed only a trace of thermal hysteresis, even at 0.96 mM protein concentration. This result was consistent with our previous experiment (*14*).

Ca^{2+}-Binding Affinity Analysis. Equilibrium dialysis was performed on all Ala mutants (Table 1) and other mutants to analyze the effects of substitutions of CaCRs on Ca^{2+}-binding affinity (data not shown). The K_d values of Ala mutants, ranging from 0.74 to 5.10 mM, were within 1−2 orders magnitude of the K_d of wild-type hAFP, suggesting that mutation of the individual coordinating residues resulted in similar decreases in Ca^{2+}-binding affinity. Double mutant E99Q/N113D showed a K_d 2.5-fold lower than that of wild-type hAFP (Table 1).

Equilibrium dialysis analysis showed an increased K_d of hAFP for Ca^{2+} when a single potential Ca^{2+}-binding residue was replaced, indicating that all five residues, Q92, D94, E99, N113, and D114, are CaCRs. The involvement of E99 as a CaCR indicates that the pattern of coordination of the CaBS in hAFP is similar to that of MBP rather than E-selectin (Figure 7) (*15*, *16*).

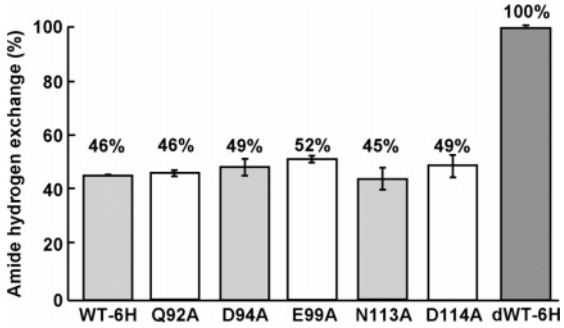

FIGURE 5: Hydrogen−deuterium exchange of hAFP and its CaCR mutants as detected by mass spectrometry. The relative exchange rate was measured as described in Experimental Procedures. dWT-6H represents the denatured wild-type hAFP WT-6H.

General Conformational Change of Ala Mutants Determined by Amide Hydrogen Exchange. To further demonstrate that the mutation at the CaBS of hAFP would not cause any dramatic conformational change, hydrogen−deuterium exchange was carried out on wild-type hAFP and the five Ala mutants of the CaCRs. The labeling process by deuterium is based on the fact that some amides and certain side chains in proteins exchange more slowly due to hydrogen-bonding interactions and sequestration from solvent. Therefore, hydrogen atoms on the surface of proteins and those not involved in the formation of the secondary and tertiary structures will exchange more rapidly. Thus, these differential exchange rates provide valuable insight into protein conformation and solvent accessibility (*24*). Hydrogen−deuterium exchange of hAFPs occurred rapidly, indicating that these proteins were well packed. No significant difference was observed in the exchange of hAFPs during a 2 h incubation, suggesting that these mutants were stable. Thus, the steady state of exchange was measured instead of monitoring the kinetic process of hydrogen exchange. As shown in Figure 5, Ala substitutions showed similar amide hydrogen exchange rates, ranging from 45% to 52%, that were comparable to 46% for wild-type hAFP, using totally deuterium-exchanged hAFP as a control. This result indicated that these Ala mutants were properly folded.

Ca^{2+}-Dependent Intrinsic Fluorescence of Ala Mutants. The fluorescence spectrum of wild-type hAFP indicated that the major fluorescence intensity was contributed by Trp residues at its maximum emission wavelength of 351 nm, a characteristic of fully exposed Trp residues (*25*). It is reasonable to assume that the change of intrinsic fluorescence intensity induced by Ca^{2+} mainly reflects the conformational change of the CaBS since we found in this study that Ca^{2+} did not cause dramatic change of the core structure of hAFP (see Discussion). Although there are seven Trp residues in hAFP, Ca^{2+}-increased fluorescence intensity could be contributed primarily by the change at the microenvironment of W112, which is the only Trp present in the Ca^{2+}-binding loop (*11*). In the fluorescence spectra of Ala mutants, there was no shift of the maximum emission wavelength, indicating that the predominantly polar character of the indole environment of W112 remained unaltered. Ca^{2+} increased the fluorescence intensity of the mutants D94A and N113A, similar to wild-type hAFP (data not shown). However, there was minimal change of the fluorescence intensity for mutants Q92A, E99A, and D114A after Ca^{2+} binding (Figure 6).

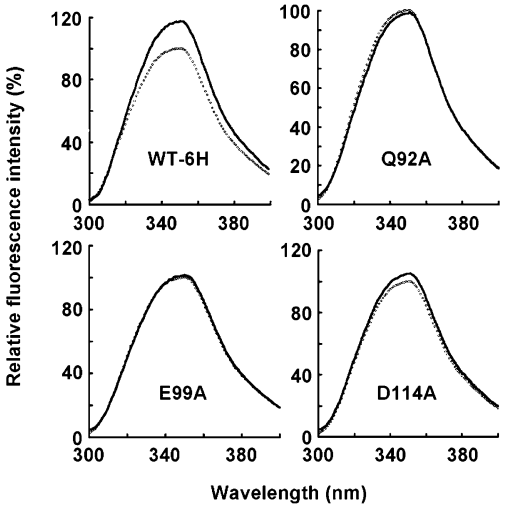

FIGURE 6: Ca^{2+}-induced intrinsic fluorescence changes of hAFP and its Ala mutants. Dashed lines represent the fluorescence spectra of apo-hAFPs, and solid lines represent the fluorescence spectra of hAFPs in the presence of Ca^{2+}.

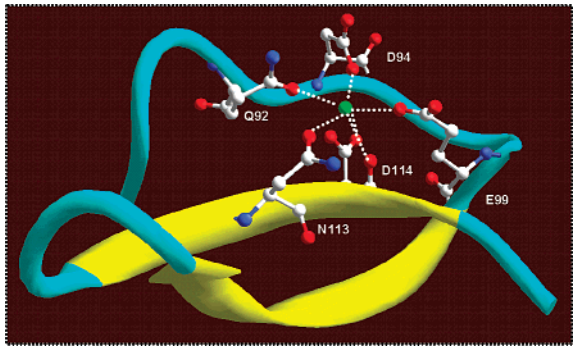

FIGURE 7: Ca^{2+}-coordinating loop of hAFP. The base of the pentagonal bipyramid coordination site of Ca^{2+} is formed by oxygen atoms from the side chains of Q92, D94, E99, and N113 and the main-chain carbonyl oxygen of D114; one apex of the bipyramid is formed by the carboxylate oxygen of D114, and the other apex is formed by the OHs of H_2O (not shown). The green sphere represents Ca^{2+}. This homologous model is generated on the basis of the crystal structure of a galactose-specific lectin from *Crotalus atrox* (PDB code 1JZN) by using the program Swiss-PdbViewer v3.7.

DISCUSSION

Structural evaluation of the CaCR mutants has demonstrated that mutation at the CaBS does not affect significantly the protein fold and the stability of hAFP. $^{45}CaCl_2$ overlay and Glu-C proteolysis protection assays revealed that all mutants preserved the Ca^{2+}-binding properties. Since hAFP contains 17 potentially susceptible acidic residues, any cleavage of these peptide bonds should provide an indication of the conformational change of hAFP and its mutants. As shown by the proteolysis protection assay, the conformational change of hAFP caused by mutation was limited upon Ca^{2+} binding, even though the binding might become weaker. Resistance of mutants E99A and D114A to proteolysis in the absence of Ca^{2+} suggested that once the cleavage sites of Glu-C at the Ca^{2+}-binding loop were altered, no further degradation occurred. It appears that Ca^{2+} binding does not cause any major changes of the lower two-thirds core structure of hAFP, a finding similar to that observed in MBP (*26*). Moreover, 1D NMR studies of a L-swap mutant of sea raven AFP with an insertion at the CaBS indicated no extensive alteration in protein fold compared to the wild-type protein (*27*). The apparent structural rigidity of the lower two-thirds portion of hAFP probably results from stabilizing interactions provided by secondary structure elements, disulfide bonds, and a well-packed hydrophobic core. Furthermore, the finding that Ca^{2+} failed to modulate the conformational changes of E99A and D114A as detected by fluorescence analysis was consistent with the results of proteolysis protection assay. This would support the speculation that the conformation of the mutants E99A and D114A in the absence of Ca^{2+} is similar to that of the Ca^{2+}-bound form, further implying that the Ala replacement would not cause dramatic change in the Ca^{2+}-binding loop region.

In this study, the weaker binding of Ca^{2+} in these mutants was likely compensated for by measuring thermal hysteresis in excess Ca^{2+}. Therefore, any significant difference in antifreeze activity among the mutants should be due to the loss of the side chains necessary for ice binding (*28*). The X-ray structure of the carbohydrate-recognition domain and its carbohydrate complex in the rat MBP has indicated that the main interaction with carbohydrate is via direct ligation to Ca^{2+} and five CaCRs (*15*). Further studies on other carbohydrate-recognition domains have shown this to be the case across the C-type lectin family (*16*, *29*, *30*). Mutagenesis of MBP also demonstrated that substitutions at six of the seven CaCRs eliminated carbohydrate binding (*13*, *28*). Unlike MBP with all five CaCRs involved in carbohydrate binding, significant loss of ice-binding activity occurred in CaCR mutants 99 and 114, suggesting that the IBS of hAFP is localized at the region defined by these two residues. Substitutions at position 114 resulted in the most severe effect on antifreeze activity and Ca^{2+} affinity. D114, which corresponds to D206 in MBP, might serve as the bidentate ligand by contributing two oxygen atoms to coordinate Ca^{2+} as D206 in MBP (Figure 7) (*15*, *31*). The relatively higher K_d for D114A, compared with other Ala mutants, supports this speculation. Therefore, D114 is critical both structurally and functionally in hAFP. Interestingly, studies of the tetranectin, a C-type lectin with a plasminogen-binding property, also demonstrated that residues corresponding to residues E99 and D114 in hAFP are important for plasminogen binding (*32*).

Ala replacements at positions Q92 and D94 failed to seriously disrupt antifreeze activity, implying these residues are not involved in ice binding directly. However, D94, a component of the Asx turn at the Ca^{2+}-binding loop, is important for stabilization of the main-chain conformation and correct positioning of the Ca^{2+}-coordinating oxygen atoms in hAFP (*33*, *34*). The nonactive mutant Q92K also indicated that the IBS of hAFP is distinguishable from the Ca^{2+}-independent type II sea raven AFP, in which the equivalent residue at position 92 is lysine (*12*). This finding confirmed that different type II AFPs use different surfaces for binding to ice even though they adopt similar protein folds.

It is presently unknown whether Ca^{2+} itself is involved in ice recognition either indirectly, by shaping the binding site, or through direct binding of ice to Ca^{2+} as in the C-type lectins (*15*). However, the CaBS of hAFP could interact with ice through a network of coordination and hydrogen bonds to provide a complementary ice-binding surface and to

stabilize the protein−ice complex, in a manner similar to that by which MBP binds to carbohydrate. Thermal hysteresis analyses of hAFPs indicated that surface complementarity provided by CaCRs is critical for ice binding. Single amino acid replacements of functionally critical residues 99 and 114 in hAFP can reduce antifreeze activity extensively, similar to mutagenesis studies on type I and type III AFPs (*35*−*39*). E99H, which contained a bulky residue that might cause steric hindrance, completely lost its activity. For residues which are close to the IBS, substitutions with longer side chains could interfere with surface complementarities between hAFP and ice significantly. In contrast to Ala replacements at positions 92 and 94, mutants with longer side chains, such as Q92K and D94E, seriously disrupted ice binding of hAFP and abolished the antifreeze activity completely. Our mutation study also suggested that preservation of the charge property of the Ca^{2+}-binding array is less important for antifreeze activity. Isoelectric alternates D94E, E99D, and D114E did not show higher antifreeze activity as compared to their nonisoelectric substitutions.

In the present work, our observations demonstrate the key role of the Ca^{2+}-binding loop and suggest that the region defined by the CaCRs E99 and D114 is critical for ice binding. The other three CaCRs, Q92, D94, and N113, do not interact with ice directly. Further structural information of hAFP and its mutants will await crystallographic studies. More detailed localization of the IBS of hAFP detected in this study will facilitate the structural and functional studies to identify more specific ice-binding residues and to understand the ice-binding mechanism of hAFP in the type II AFPs.

ACKNOWLEDGMENT

We thank Dr. Avijit Chakrabartty for assistance with fluorescence spectroscopy and Mr. Shashikant Joshi and Ms. Yen Ling Cho for critical reading of the manuscript.

REFERENCES

1. Fletcher, G. L., Hew, C. L., and Davies, P. L. (2001) Antifreeze proteins of teleost fishes, *Annu. Rev. Physiol. 63*, 359−390.
2. Davies, P. L., and Sykes, B. D. (1997) Antifreeze proteins, *Curr. Opin. Struct. Biol. 7*, 828−834.
3. Knight, C. A., Cheng, C. C., and DeVries, A. L. (1991) Adsorption of alpha-helical antifreeze peptides on specific ice crystal surface planes, *Biophys. J. 59*, 409−418.
4. Wierzbicki, A., Taylor, M. S., Knight, C. A., Madura, J. D., Harrington, J. P., and Sikes, C. S. (1996) Analysis of shorthorn sculpin antifreeze protein stereospecific binding to (2−10) faces of ice, *Biophys. J. 71*, 8−18.
5. Knight, C. A., Driggers, E., and DeVries, A. L. (1993) Adsorption to ice of fish antifreeze glycopeptides 7 and 8, *Biophys. J. 64*, 252−259.
6. Slaughter, D., Fletcher, G. L., Ananthanarayanan, V. S., and Hew, C. L. (1981) Antifreeze proteins from the sea raven, *Hemitripterus americanus*. Further evidence for diversity among fish polypeptide antifreezes, *J. Biol. Chem. 256*, 2022−2026.
7. Ewart, K. V., and Fletcher, G. (1990) Isolation and characterization of antifreeze proteins from smelt (*Osmerus mordax*) and atlantic herring (*Clupea harengus harengus*), *Can. J. Zool. 68*, 1652−1658.
8. Ewart, K. V., and Fletcher, G. L. (1993) Herring antifreeze protein: primary structure and evidence for a C-type lectin evolutionary origin, *Mol. Mar. Biol. Biotechnol. 2*, 20−27.
9. Ewart, K. V., Rubinsky, B., and Fletcher, G. L. (1992) Structural and functional similarity between fish antifreeze proteins and calcium-dependent lectins, *Biochem. Biophys. Res. Commun. 185*, 335−340.
10. Drickamer, K. (1999) C-type lectin-like domains, *Curr. Opin. Struct. Biol. 9*, 585−590.
11. Ewart, K. V., Yang, D. S., Ananthanarayanan, V. S., Fletcher, G. L., and Hew, C. L. (1996) Ca^{2+}-dependent antifreeze proteins. Modulation of conformation and activity by divalent metal ions, *J. Biol. Chem. 271*, 16627−16632.
12. Loewen, M. C., Gronwald, W., Sönnichsen, F. D., Sykes, B. D., and Davies, P. L. (1998) The ice-binding site of sea raven antifreeze protein is distinct from the carbohydrate-binding site of the homologous C-type lectin, *Biochemistry 37*, 17745−17753.
13. Drickamer, K. (1992) Engineering galactose-binding activity into a C-type mannose-binding protein, *Nature 360*, 183−186.
14. Ewart, K. V., Li, Z., Yang, D. S., Fletcher, G. L., and Hew, C. L. (1998) The ice-binding site of Atlantic herring antifreeze protein corresponds to the carbohydrate-binding site of C-type lectins, *Biochemistry 37*, 4080−4085.
15. Weis, W. I., Drickamer, K., and Hendrickson, W. A. (1992) Structure of a C-type mannose-binding protein complexed with an oligosaccharide, *Nature 360*, 127−134.
16. Graves, B. J., Crowther, R. L., Chandran, C., Rumberger, J. M., Li, S., Huang, K. S., Presky, D. H., Familletti, P. C., Wolitzky, B. A., and Burns, D. K. (1994) Insight into E-selectin/ligand interaction from the crystal structure and mutagenesis of the lec/EGF domains, *Nature 367*, 532−538.
17. Aiyar, A., and Leis, J. (1993) Modification of the megaprimer method of PCR mutagenesis: improved amplification of the final product, *BioTechniques 14*, 366−368.
18. Li, Z., Xiong, F., Lin, Q., d'Anjou, M., Daugulis, A. J., Yang, D. S. C., and Hew, C. L. (2001) Low-temperature increases the yield of biologically active herring antifreeze protein in *Pichia pastoris*, *Protein Expression Purif. 21*, 438−445.
19. Mach, H., Middaugh, C. R., and Lewis, R. V. (1992) Statistical determination of the average values of the extinction coefficients of tryptophan and tyrosine in native proteins, *Anal. Biochem. 200*, 74−80.
20. Maruyama, K., Mikawa, T., and Ebashi, S. (1984) Detection of calcium binding proteins by ^{45}Ca autoradiography on nitrocellulose membrane after sodium dodecyl sulfate gel electrophoresis, *J. Biochem. 95*, 511−519.
21. Chakrabartty, A., Yang, D. S., and Hew, C. L. (1989) Structure−function relationship in a winter flounder antifreeze polypeptide. II. Alteration of the component growth rates of ice by synthetic antifreeze polypeptides, *J. Biol. Chem. 264*, 11313−11316.
22. Hillig, W. B., and Turnbull, D. (1956) Theory of crystal growth in an undercooled pure liquid, *J. Chem. Phys. 24*, 912.
23. Chao, H., DeLuca, C. I., and Davies, P. L. (1995) Mixing antifreeze protein types changes ice crystal morphology without affecting antifreeze activity, *FEBS Lett. 357*, 183−186.
24. Hvidt, A. (1996) Hydrogen exchange in proteins, *Adv. Protein Chem. 21*, 287−385.
25. Eftink, M. R. (1990) Fluorescence techniques for studying protein structure, *Methods Biochem. Anal. 35*, 117−129.
26. Ng, K. K., and Weis, W. I. (1998) Coupling of prolyl peptide bond isomerization and Ca^{2+} binding in a C-type mannose-binding protein, *Biochemistry 37*, 17977−17989.
27. Loewen, M. C., Chao, H., Houston, M. E., Jr., Baardsnes, J., Hodges, R. S., Kay, C. M., Sykes, B. D., Sönnichsen, F. D., and Davies, P. L. (1999) Alternative roles for putative ice-binding residues in type I antifreeze protein, *Biochemistry 38*, 4743−4749.
28. Quesenberry, M. S., and Drickamer, K. (1992) Role of conserved and nonconserved residues in the Ca^{2+}-dependent carbohydrate-recognition domain of a rat mannose-binding protein. Analysis by random cassette mutagenesis, *J. Biol. Chem. 267*, 10831−10841.
29. Poget, S. F., Legge, G. B., Proctor, M. R., Butler, P. J., Bycroft, M., and Williams, R. L. (1999) The structure of a tunicate C-type lectin from Polyandrocarpa misakiensis complexed with D-galactose, *J. Mol. Biol. 290*, 867−879.
30. Meier, M., Bider, M. D., Malashkevich, V. N., Spiess, M., and Burkhard, P. (2000) Crystal structure of the carbohydrate recognition domain of the H1 subunit of the asialoglycoprotein receptor, *J. Mol. Biol. 300*, 857−865.
31. Drickamer, K. (1996) Ca^{2+}-dependent sugar recognition by animal lectins, *Biochem. Soc. Trans. 24*, 146−150.
32. Graversen, J. H., Lorentsen, R. H., Jacobsen, C., Moestrup, S. K., Sigurskjold, B. W., Thogersen, H. C., and Etzerodt, M. (1998) The plasminogen binding site of the C-type lectin tetranectin is

located in the carbohydrate recognition domain, and binding is sensitive to both calcium and lysine, *J. Biol. Chem. 273*, 29241−29246.
33. Rees, D. C., Lewis, M., and Lipscomb, W. N. (1983) Refined crystal structure of carboxypeptidase A at 1.54 Å resolution, *J. Mol. Biol. 168*, 367−387.
34. Baker, E. N., and Hubbard, R. E. (1984) Hydrogen bonding in globular proteins, *Prog. Biophys. Mol. Biol. 44*, 97−179.
35. Wen, D., and Laursen, R. A. (1992) Structure−function relationships in an antifreeze polypeptide. The role of neutral, polar amino acids, *J. Biol. Chem. 267*, 14102−14108.
36. Chao, H., Sönnichsen, F. D., DeLuca, C. I., Sykes, B. D., and Davies, P. L. (1994) Structure−function relationship in the globular type III antifreeze protein: identification of a cluster of surface residues required for binding to ice, *Protein Sci. 3*, 1760−1769.
37. Jia, Z., DeLuca, C. I., Chao, H., and Davies, P. L. (1996) Structural basis for the binding of a globular antifreeze protein to ice, *Nature 384*, 285−288 [erratum: Jia, Z., DeLuca, C. I., Chao, H., and Davies, P. L. (1997) *Nature 385*, 555].
38. Chao, H., Houston, M. E., Jr., Hodges, R. S., Kay, C. M., Sykes, B. D., Loewen, M. C., Davies, P. L., and Sönnichsen, F. D. (1997) A diminished role for hydrogen bonds in antifreeze protein binding to ice, *Biochemistry 36*, 14652−14660.
39. Wen, D., and Laursen, R. A. (1992) A model for binding of an antifreeze polypeptide to ice, *Biophys. J. 63*, 1659−1662.

BI048485H